Supporting Information

Christie et al. 10.1073/pnas.1116975109

SI Materials and Methods

Protein Production. PCR fragments of Sx1a (residues 1–261) and Sx1aΔN (residues 25–261) were generated by amplification of a codon-optimized synthetic Sx1a gene (GeneArt). PCR fragments of Sx4ΔN (residues 30–275) were generated by amplification of Sx4-C141S (residues 1–275). All fragments were cloned into the pET24a expression vector, yielding C-terminally His-tagged Sx constructs. Munc18c (residues 1–592), C-terminally His-tagged Sx4-C141S (residues 1–275) and N-terminally GST-tagged and C-terminally His-tagged constructs of Munc18-1 are described elsewhere (1, 2). Munc18c was expressed as an N-terminally His-tagged protein in baculovirus-infected insect cells (1). All unlabeled proteins were expressed in BL21(DE3)pLysS cells in autoinduction media ZYP-5052 (3). Proteins were purified as described elsewhere (1, 2). The formation of a 1:1 complex was assessed by size exclusion chromatography: Munc18:Sx complexes eluted at the predicted position for a 100-kDa complex, the expected molecular mass of the 1:1 complex.

ITC. ITC experiments were carried out at 298 K using an iTC_{200} (Microcal). Munc18-1 at 5–7 μM was titrated with Sx1 or Sx1ΔN at 50–70 μM using 2.45-μL injections, whereas Munc18c at 5–20 μM was titrated with 90–250 μM Sx4 or Sx4ΔN using 3.1-μL injections. Microcal ORIGIN 7 software was used to integrate the heat released and calculate the binding enthalpy (ΔH), equilibrium constant K_a ($1/K_d$), and stoichiometry (N). The Gibbs free energy (ΔG) was calculated using the equation: $\Delta G = -RT\ln(K_a)$; binding entropy (ΔS) was calculated using $\Delta G = \Delta H - T\Delta S$. Each experiment was performed in triplicate, and the reported parameters are the average and SD of values determined from each of the three experiments (Fig. S1 and Table S1).

Protein Deuteration. Deuterium-labeled Sx4-C141S (residues 1–275) (^{D}Sx4) was produced from cultures of M9 salts minimal media containing 99% D_2O and unlabeled glucose. After transformation into BL21(DE3) pLysS, cells were adapted for growth in deuterated media by inoculating minimal media containing 50% D_2O with a single colony. When the optical density at 600 nm (OD_{600}) reached 1.0, this culture was used to inoculate media containing 70% D_2O at OD_{600} of 0.1. This process was repeated for minimal media containing 90% and then 99% D_2O. Preparative cultures of ^{D}Sx4 were inoculated at OD_{600} of 0.01 and induced at mid exponential phase (OD_{600}, 0.5–0.6) with 1 mM IPTG. Protein expression was carried out at 37 °C for 24 h, and yielded ∼1 mg of purified protein/L of culture. The incorporation of deuterium in ^{D}Sx4 was determined by MALDI-TOF mass spectrometry using a Voyager DE mass spectrometer (Applied Biosystems). Both Sx4 and ^{D}Sx4 were desalted using C18 Zip-tips (Millipore) and prepared for analysis by mixing 0.5 μL of the desalted protein in 50% acetonitrile, 0.1% formic acid to 0.5 μL of matrix (10 mg/mL of sinapinic acid in 60% acetonitrile, 0.1% formic acid). Samples were spotted onto a MALDI plate and allowed to air dry before MS spectra were collected. The deuteration level was determined to be ∼85% by comparison of Sx4 and ^{D}Sx4 spectra.

Deuterium-labeled Sx1a (residues 1–265) (^{D}Sx1a) was produced at the Australian Deuteration Facility from cultures grown in "ModC1" (4) containing 90% D_2O (vol/vol) and unlabeled glycerol (40 g/L). Miniprep plasmid DNA pET24a-Sx1a was used to transform 50 μL of Invitrogen supercompetent BL21*(DE3) cells, which was then incubated with 250 μL of SOC for 2 h. The 300-μL culture was transferred to 10 mL ModC1 media containing 50% D_2O, shaking at 200 rpm, 37 °C. After 11 h (OD_{600}, 0.11), 9 mL was added to 36 mL fresh media at 100% D_2O (thus producing 45 mL at 90% D_2O). After another 12 h (OD_{600}, 1.288), the culture (minus samples, i.e., total volume ∼40 mL) was used to inoculate 1 L of fresh media in a 2L Real Time Engineering bioreactor, aerated with air at 0.5 L/min, and with pH held to 7.0 by addition of 28% NH_4OH in H_2O (Sigma). Dissolved oxygen tension was maintained above 30% at all times. The culture grew with a doubling time of ∼5 h. At 33 h, the temperature was lowered from 37 °C to 30 °C. At 34 h (OD_{600}, 16.5) expression was induced by the addition of 5 mM IPTG. After 5 h, (OD_{600}, 37.2) the culture was harvested with a wet weight yield of 56.6 g with excellent expression evident by SDS-PAGE. The deuteration level was determined by MALDI-TOF comparison of unlabeled and labeled samples and was found to be ∼76%. The overall yield of deuterated Sx1a was ∼20 mg of purified protein per liter of culture. Measurement of deuterated Sx1a research was facilitated by access to the Sydney University Proteome Research Unit established under the Major National Research Facilities Program of the Australian Government and supported by the University of Sydney.

Pull-Down Assays. Pull-down assays were carried out using GST-cleaved Munc18-1 (2) and His_6-cleaved Munc18c (1). Sx1 and Sx1ΔN and Sx4 and Sx4ΔN were incubated with Munc18-1 and Munc18c respectively at 4 °C for two hours. Samples were then incubated with Co^{2+} affinity beads at 4 °C for 90 min in binding buffer [25 mM Tris-HCl (pH 8), 150 mM NaCl, 10% glycerol, 15 mM imidazole, 0.1% triton X-100, and 2 mM β-mercaptoethanol]. Beads were then washed four times with binding buffer and samples of beads were analyzed by reducing SDS/PAGE stained with Coomassie Blue.

CD Spectroscopy. CD spectra for Sx4 (6 mg/mL) and Sx4ΔN (5.3 mg/mL) in 25 mM Hepes (pH 8), 200 mM NaCl, 10% glycerol, and 2 mM β-mercaptoethanol were acquired using a JASCO 810 spectropolarimeter at room temperature. Spectra were collected in a 1 mm quartz cuvette (Hellma; 100-1-40-QS) using a step size of 0.1 nm, a data pitch of 0.1 nm, and a scanning speed of 50 nm/min between 190 and 245 nm. Data presented in Fig. S2 are averages of five scans.

Differential Scanning Fluorimetry. Thermal unfolding of Sx4ΔN was assessed using differential scanning fluorimetry, which relies on the preferential binding of a fluorophore to unfolded protein (5). Thermal denaturation was carried out using a 7900 RT-PCR instrument (Applied Biosystems). Freshly prepared SYPRO orange dye (at 5,000×) (Invitrogen) was diluted in DMSO to 500× and added to protein (at 15 mg/mL) to a final concentration of 10× Sypro Orange. Relative fluorescence units (R.F.U.) were measured at the ROX dye calibration setting ($\lambda_{excitation}$, 492 nm; $\lambda_{emission}$, 610 nm) at 2 °C increments. Experiments were performed twice, with three or four replicates, and R.F.U. values averaged at each temperature.

Chemical Cross-Linking. Munc18c:Sx4 complex at 1.2 μM in 50 mM Hepes buffer (pH 7.5) was reacted with 250 μM dithiobis(sulfosuccinimidyl propionate) (DTSSP) (Pierce) for 4 min, and then Tris-HCl at pH 8.5 was added to a concentration of 0.1 M. The reaction was allowed to proceed for 20 min, and the solution was then made 50 mM in iodoacetamide and allowed to react for another 30 min in the dark. The sample was then run on non-reducing SDS/PAGE and subjected to in-gel tryptic digestion

(Promega sequencing grade trypsin). The digest was fractionated on an Agilent 1100 nano-HPLC system and cross-links were identified using MALDI TOF/TOF using a 4700 Proteomics Analyzer from Applied Biosystems, and the assignment of cross-linked peptides was made as described in King et al. (6).

To expand the number of crosslinks, we also used BS3 in combination with reductive alkylation, with MALDI and ESI MS analysis. Munc18c:Sx4 complex at ~2 μM in 25 mM Hepes (pH 7), 300 mM NaCl, 10% glycerol, and 2 mM DTT was reacted with 62 mM iodoacetamide at room temperature in the dark for 30 min. The solution was then made up to a concentration of 690 μM of the cross-linker bis(sulfosuccinimidyl) suberate (BS3; Pierce) and incubated for a further 30 min before the reaction was stopped by the addition of 50 mM NH_4CO_3 (pH 8.0). The sample was concentrated to ~50 μM protein, digested with 7.5 μg of trypsin, and 75 μL of this solution was incubated on ice overnight with 8 μL of 1 M formaldehyde and 4 μL of 1 M dimethylamine-borane complex for reductive methylation. Methylated peptides were desalted using C18 Zip-tips (Millipore) and analyzed by liquid chromatography electrospray ionization mass spectrometry (LC ESI-MS) using an Agilent 1100 nano-HPLC and a QSTAR Elite mass spectrometer (Applied Biosystems). The assignment of cross-linked peptides was made based on precursor *m/z* (the intact cross-link MH+), the partial sequence of at least one of the peptides and the presence of *a* ions corresponding to the dimethylated N-terminal amino acids of both peptides (7).

Munc18-1:Sx1a complex at ~6 μM in 25 mM Hepes (pH 8), 200 mM NaCl, 10% glycerol, and 2 mM DTT was reacted with 45 mM iodoacetamide at room temperature in the dark for 30 min. The solution was then made up to a concentration of 690 μM of the cross-linker BS3 (Pierce), which was composed of equal quantities of undeuterated BS3 and deuterated BS3(d4), and incubated for a further 15 min before the reaction was stopped by the addition of 50 mM NH_4CO_3 (pH 8.0). The sample was buffer exchanged into 50 mM NH_4CO_3 pH 8.0, concentrated to ~12 μM protein and digested with 15 μg trypsin (Promega) overnight at 37 °C. The sample was then lyophilized and dissolved in 0.1% formic acid.

The digested sample was analyzed on LC-ESI-MS on a Shimadzu Nexera Ultra HPLC coupled to a TripleTOF 5600 mass spectrometer (ABSCIEX, Canada) equipped with a duo electrospray ion source. Three microliters of each extract were injected onto a 2.1 × 100 mm Zorbax C18 1.8-μm column (Agilent) at 400 μL/min. Linear gradients of 1–40% solvent B over 25 min at 400 μL/min flow rate, followed by a steeper gradient from 40 to 80% solvent B in 15 min were used for peptide elution. Solvent B was held at 80% for 5 min for washing the column and returned to 1% solvent B for equilibration before the next sample injection. Solvent A consisted of 0.1% formic acid (aqueous) and solvent B contained 90/10 acetonitrile/0.1% formic acid (aqueous). The ion spray voltage was set to 5,300 V, declustering potential (DP) 100 V, curtain gas flow 25, nebulizer gas 1 (GS1) 25, GS2 to 35, interface heater at 150 °C, and the turbo heater to 450 °C. The mass spectrometer acquired 250-ms full-scan TOF-MS data, and each TOF-MS scan was followed by 20 sets of 50-ms full-scan product ion data in an Information Dependent Acquisition (IDA) mode. Full-scan TOFMS data were acquired over the mass range 350–1,800 and for product ion MS/MS 100–1,800. Ions observed in the TOF-MS scan exceeding a threshold of 200 counts and a charge state of +2 to +5 were set to trigger the acquisition of product ion, MS/MS spectra of the resultant 20 most intense ions. The data were acquired and processed using Analyst TF 1.5.1 software (ABSCIEX).

The assignment of cross-linked peptides was made based on precursor *m/z* (the intact cross-link MH+), the partial sequence of at least one of the peptides and the presence of a deuterated MH+ partner 4-Da higher in mass.

Modeling of Complexes Against Scattering and Cross-Linking Data. Crystal structures of Munc18-1, Munc18c and Sx1a have disordered regions that are not modeled. In addition there is no crystal structure of Sx4. The i-TASSER server (8) uses information from the Protein Data Bank and structural optimizations to build homology structures based on sequence. As the templates for Munc18-1, Munc18c, and Sx1a were essentially complete, i-TASSER was used to build missing regions including the C-terminal histidine tag of Sx1a. i-TASSER predicts the extension to be helical, and these residues were therefore modeled as helical in the refinements. For Sx4, i-TASSER was used to build a homology model based largely upon the Sx1a crystal structure. The only change that was made to the i-TASSER generated structures was to extend domain 3a of Munc18-1 and Munc18c into a helical hairpin using Pymol (9), in agreement with crystal structures of Munc18-1:Sx4 N-peptide [Protein Data Bank (PDB) ID code 3PUJ] (2) and Munc18c:Sx4 N-peptide (PDB ID code 2PJX) (10).

For the purposes of rigid body modeling against the scattering data, the Munc18:Sx structures were broken into 8 groups. For Munc18-1:Sx1a, the groups were: Munc18-1(1-135) (domain 1); Munc18-1(136-594) (domains 2 and 3); Sx1a(1-10) (N-peptide); Sx1a(11-29) (flexible loop); Sx1a(30-160) (Habc); Sx1a(161-181) (linker); Sx1a(182-232) (H3a); Sx1a(233-247) (H3b); and Sx1a (248-267) (H3c). For Munc18c:Sx4, the groups were: Munc18c(1-138) (domain 1); Munc18c(139-592) (domains 2 and 3); Sx4(1-10) (N-peptide); Sx4(11-34) (flexible loop); Sx4(35-168) (Habc); Sx4 (169-189) (linker); Sx4(190-240) (H3a); Sx4(241-255) (H3b); and Sx4(256-275) (H3c). The justification for splitting Munc18 into two rigid units was based on the observation by Hu et al. (2) and Bracher and Weissenhorn (11) that domain 1 of Munc18-1 and squid Sec1 can rotate with respect to domains 2 and 3 by at least 23°. The Sx proteins were broken into seven groups on the basis of observed rigid and flexible regions in the crystal structure of Sx1a complexed with Munc18-1. The relative positions of Munc18 domain 1 and the N-peptide of Sx were fixed and the positions of the remaining 7 units were refined against the scattering data.

Cross-links were included in the optimization as restraints, as indicated in Table S4. Depending on the cross-linking compound used, the distance between α-carbons is between 27–28 Å. However, some cross-links are formed between flexible loops that are forced to be rigid in the modeling process, so 35 Å was used as the maximum distance between cross-linked residues. In addition to cross-link restraints, the Sx H3 domain (specifically the region residues 226–240 in Sx1a or the homologous region in Sx4, residues 234–248) was restrained to make at least one contact (<15 Å) with Munc18. This last restraint was added because several cross-links were identified between Munc18c and Sx4 H3 but not used in refinement, because they indicated flexibility in Sx4 H3c (Table S4) and because ITC data showed that Sx1a-(1-240) binds Munc18-1 with almost equal affinity as Sx1a-(1-260) but that Sx1a-(1-226) binds much more weakly (12).

Rigid body modeling was performed with SASREF7 (13) by simultaneous optimization against the SAXS data and the neutron contrast variation datasets. In each case, data between q = 0.015–0.25 $Å^{-1}$ and the distance restraints described above were included in the modeling procedure. SASREF7 was run 10 times, and the model that represented the best fit (as judged by the fit parameter calculated by SASREF) to the data were chosen as the model of the Munc18:Sx complex.

The positioning of the Sx4 H3 helix is not precise in the models; without its native membrane anchor, the C terminus of Sx4 is flexible. For example, the cross-linking experiments suggest that lysine residues at the C terminus of Sx4 are proximal to K516 and T519 on Munc18c. However, these cross-links are not consistent with the scattering data of the complex. The likely reason for this is that the H3 helix samples a range of conformations, and some transient conformations may be trapped by cross-linking. There is

also a deviation between the model and the 100% D_2O scattering data at low angle. The 100% data are dominated by scattering from the Munc18c protein; therefore, it is probable that the Munc18c structure we used to model the scattering data are not sufficiently flexible. For example, loop regions such as residues 487–530 and domain 3a are known to be flexible (2, 10, 14) and may not be modeled correctly in the template structure. Rather than increase the number of variables for modeling and possibly overfit the data, we took the decision to keep the number of variables to a minimum and so did not specifically incorporate flexibility in these two regions.

Calculation of Scattering Profiles from Crystal Structures. The program CRYSOL (15) was used to calculate the X-ray scattering profile from the crystal structure of the Munc18-1:Sx1a complex (PDB ID code 3C98) (12), to compare it to the small-angle scattering data from the Munc18-1:Sx1a and Munc18-1:Sx1aΔN complexes and to calculate the structural parameters presented in Table 1. The program CRYSON (16) was used to calculate structural parameters for the Munc18-1:Sx1a crystal structure in 40% and 100% D_2O.

Dynamic Light Scattering. Dynamic light scattering data were measured for solution complexes of M18-1:Sx1a (0.5 mg/mL) and M18-1:Sx1aΔN (0.3 mg/mL) in 25 mM Hepes (pH 7), 300 mM NaCl, and 2 mM β-mercaptoethanol on a Zetasizer Nano ZS instrument (Malvern Instruments). Samples were centrifuged at 10,000 × *g* for 5 min before measurement. Experiments were performed at 22 °C using a cuvette with a path length of 1 cm. An average of three acquisitions was used for analysis. Analysis was performed using Zetasizer software (Malvern Instruments).

1. Hu SH, et al. (2003) Recombinant expression of Munc18c in a baculovirus system and interaction with syntaxin4. *Protein Expr Purif* 31:305–310.
2. Hu SH, et al. (2011) Possible roles for Munc18-1 domain 3a and Syntaxin1 N-peptide and C-terminal anchor in SNARE complex formation. *Proc Natl Acad Sci USA* 108: 1040–1045.
3. Studier FW (2005) Protein production by auto-induction in high density shaking cultures. *Protein Expr Purif* 41:207–234.
4. Middelberg AP, O'Neill BK, L Bogle ID, Snoswell MA (1991) A novel technique for the measurement of disruption in high-pressure homogenization: Studies on E. coli containing recombinant inclusion bodies. *Biotechnol Bioeng* 38:363–370.
5. Niesen FH, Berglund H, Vedadi M (2007) The use of differential scanning fluorimetry to detect ligand interactions that promote protein stability. *Nat Protoc* 2:2212–2221.
6. King GJ, et al. (2008) Identification of disulfide-containing chemical cross-links in proteins using MALDI-TOF/TOF-mass spectrometry. *Anal Chem* 80:5036–5043.
7. Hsu JL, Huang SY, Shiea JT, Huang WY, Chen SH (2005) Beyond quantitative proteomics: Signal enhancement of the a1 ion as a mass tag for peptide sequencing using dimethyl labeling. *J Proteome Res* 4:101–108.
8. Zhang Y (2008) I-TASSER server for protein 3D structure prediction. *BMC Bioinformatics* 9:40.
9. DeLano WL (2002) *The Pymol User's Manual* (De Lano Scientific, San Carlos, CA).
10. Hu SH, Latham CF, Gee CL, James DE, Martin JL (2007) Structure of the Munc18c/Syntaxin4 N-peptide complex defines universal features of the N-peptide binding mode of Sec1/Munc18 proteins. *Proc Natl Acad Sci USA* 104:8773–8778.
11. Bracher A, Weissenhorn W (2001) Crystal structures of neuronal squid Sec1 implicate inter-domain hinge movement in the release of t-SNAREs. *J Mol Biol* 306:7–13.
12. Burkhardt P, Hattendorf DA, Weis WI, Fasshauer D (2008) Munc18a controls SNARE assembly through its interaction with the syntaxin N-peptide. *EMBO J* 27:923–933.
13. Petoukhov MV, Svergun DI (2005) Global rigid body modeling of macromolecular complexes against small-angle scattering data. *Biophys J* 89:1237–1250.
14. Misura KMS, Scheller RH, Weis WI (2000) Three-dimensional structure of the neuronal-Sec1-syntaxin 1a complex. *Nature* 404:355–362.
15. Svergun D, Barberato C, Koch MHJ (1995) CRYSOL - A program to evaluate x-ray solution scattering of biological macromolecules from atomic coordinates. *J Appl Cryst* 28:768–773.
16. Svergun DI, et al. (1998) Protein hydration in solution: Experimental observation by x-ray and neutron scattering. *Proc Natl Acad Sci USA* 95:2267–2272.

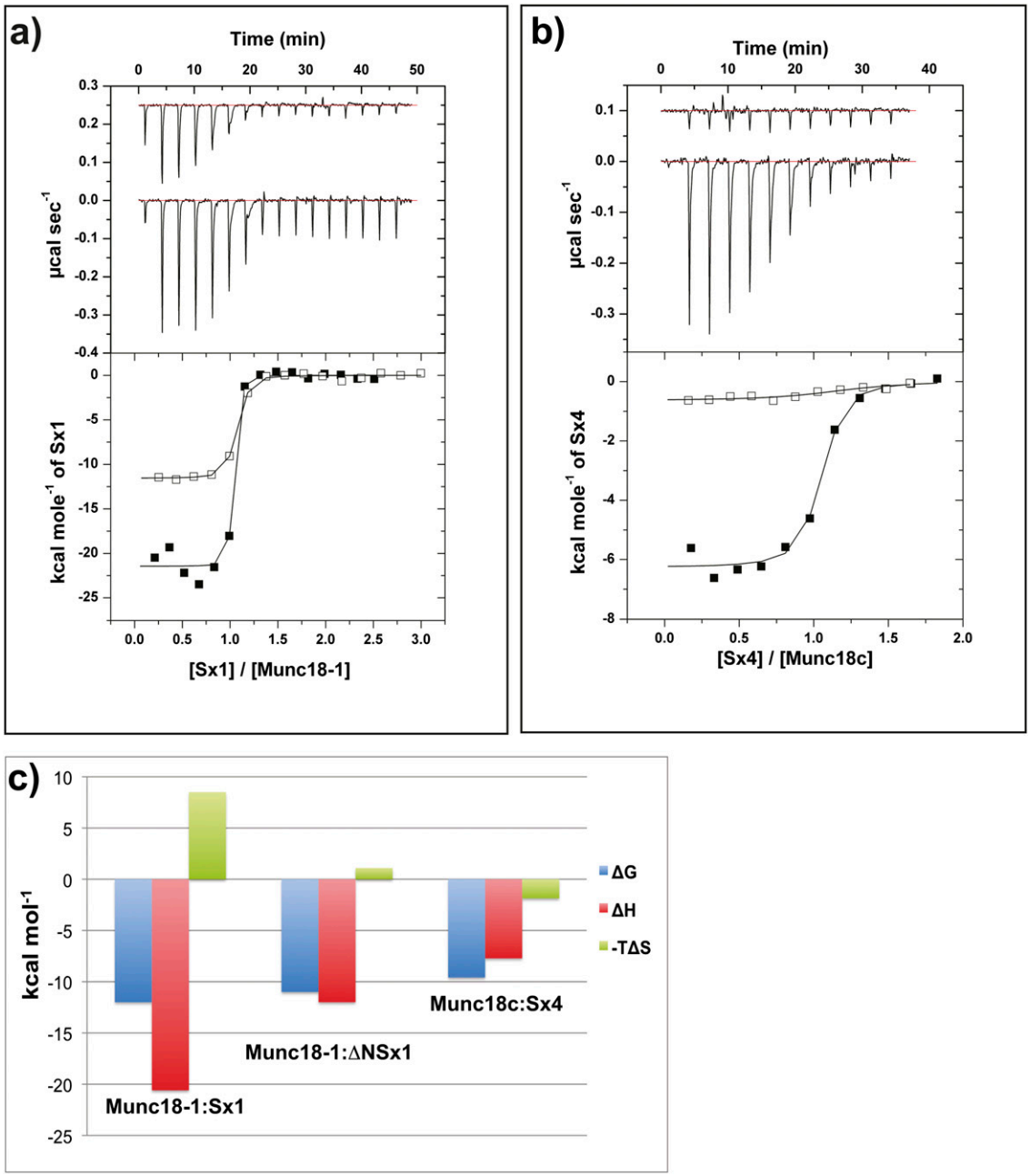

Fig. S1. ITC data for interactions between Munc18s and Sxs. (*A*) Munc18-1 and Sx1a (filled squares) and Munc18-1 and Sx1aΔN (empty squares). (*B*) Munc18c and Sx4 (filled squares) and Munc18c and Sx4ΔN (empty squares). (*C*) Comparison of the thermodynamic parameters determined from the ITC experiments.

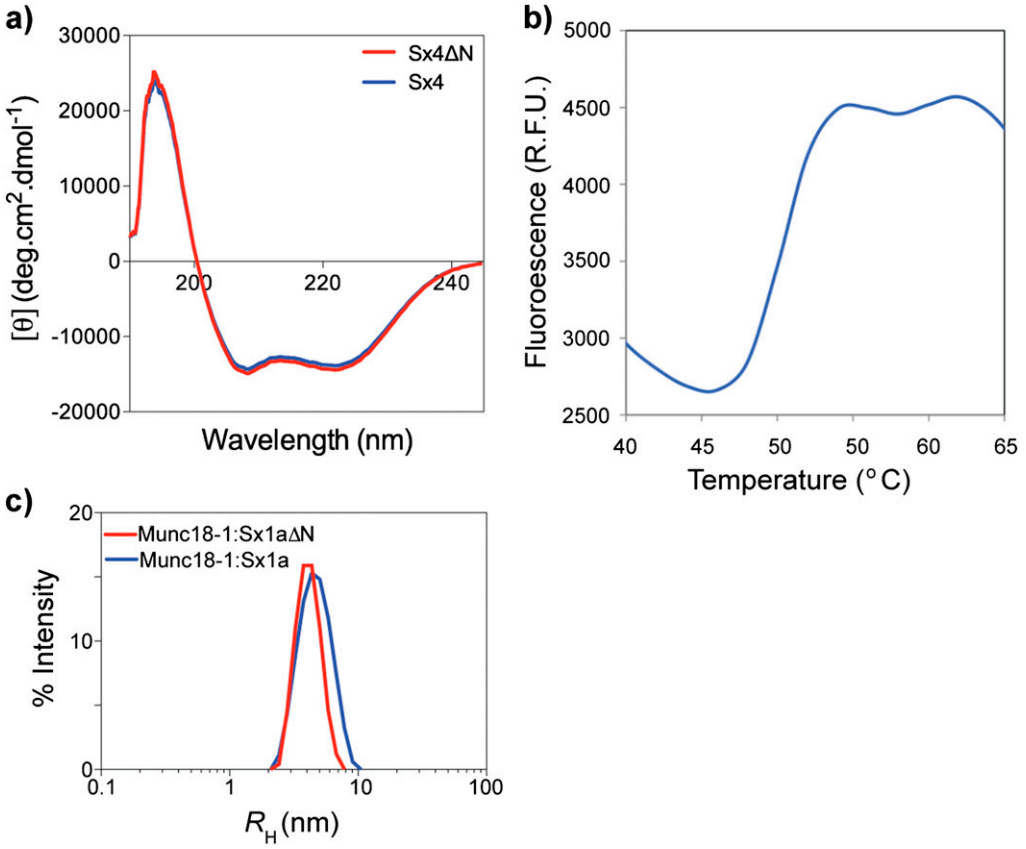

Fig. S2. Characterization of samples. (*A*) Circular dichroism spectra for Sx4 (red) and Sx4ΔN (blue), showing that the two proteins are helical. (*B*) Temperature dependent unfolding of Sx4ΔN assessed by differential scanning fluorimetry (blue). The sigmoidal curve is characteristic of cooperative thermal denaturation of a folded protein. (*C*) Dynamic light scattering confirms Munc18-1:Sx1a and Munc18-1:Sx1aΔN have different R_g values. The measured hydrodynamic radius R_H for Munc18-1:Sx1a and M18-1:Sx1aΔN was ∼48 Å and 42 Å, respectively. Converting these to R_g values using a factor of 1.25 (1) yields values for Munc18-1:Sx1a and Munc18-1:Sx1aΔN of ∼38.4 and ∼33.6 Å, respectively. These are in very good agreement with the R_g values obtained from X-ray scattering data of these complexes (38–39 and 33 Å for M18-1:Sx1a and M18-1:Sx1aΔN, respectively; see Table S2), providing independent evidence that the M18-1:Sx1a complex is larger than that of M18-1:Sx1aΔN.

1. Khurana R, Uversky VN, Nielsen L, Fink AL (2001) Is Congo red an amyloid-specific dye? *J Biol Chem* 276:22715–22721.

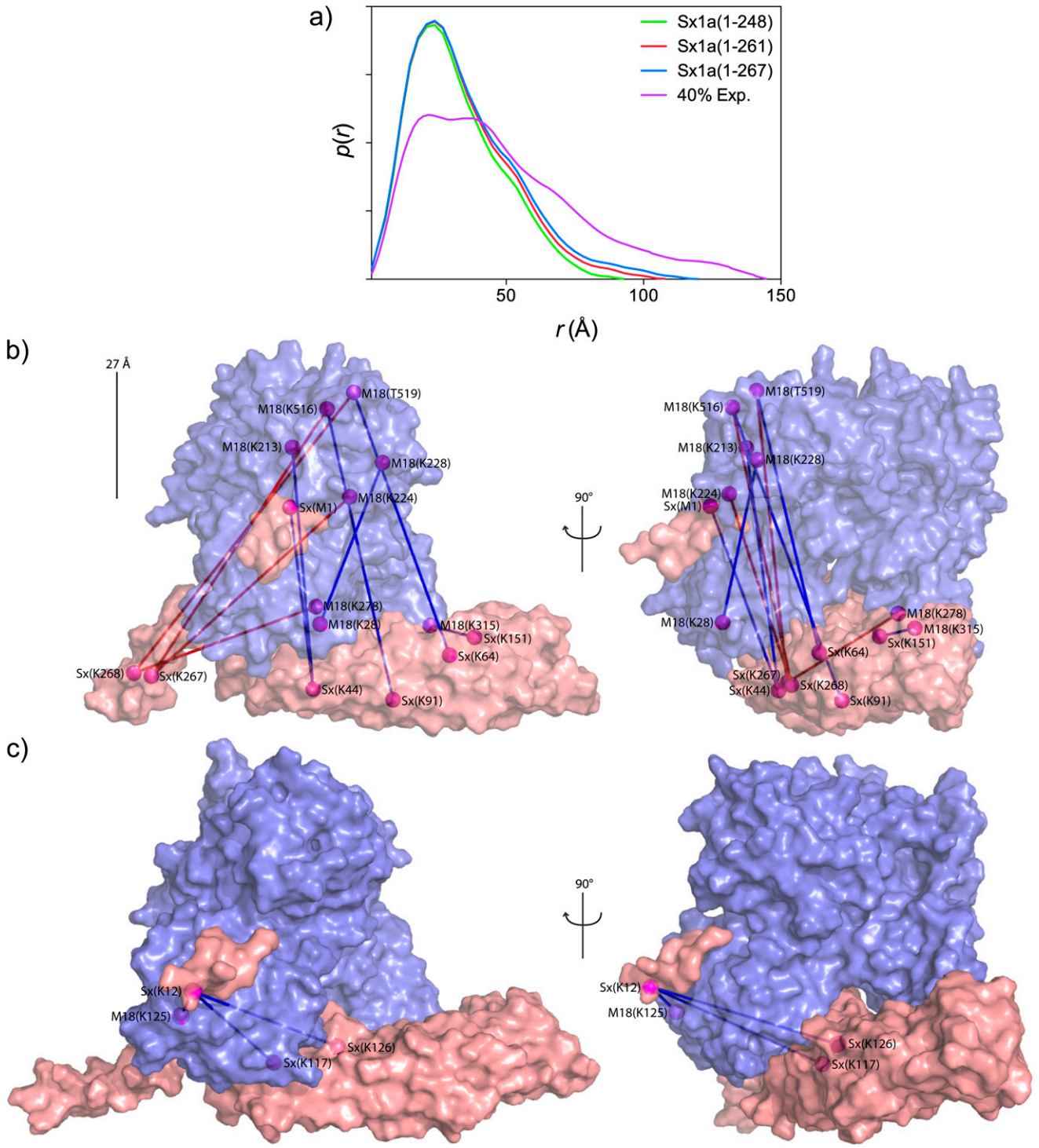

Fig. S3. Comparison of Munc18-1:Sx1a crystal structure with SANS and cross-link data. (*A*) To address the question of whether the SANS data could be explained by using a model of closed Sx1a with an extended C-terminal tail we generated closed conformation models of Sx1a(1-248), (1-261), and (1-267) and calculated the $p(r)$ distribution for each. These were compared with the experimental $p(r)$ distribution from the 40% neutron contrast variation data that represents Sx1a bound to Munc18-1 in solution (with Munc18-1 matched out). The area under the $p(r)$ curve is related to the size of the protein and the experimental curve was therefore normalized to the same area as Sx1a(1-267) for this comparison. The curves derived from the three closed models (green, red, and blue, respectively) are very similar, with increasingly longer tails for the longer constructs, and differ significantly from the experimental curve. A major difference is the presence of a second peak in the experimental $p(r)$ curve (purple): this is indicative of two domains with centers of mass separated by ∼40 Å. A second major difference is that the mass of the extended region in the experimental data is much larger than 20 residues. This is demonstrated by the larger area under the $p(r)$ curve from r ∼50 Å onward. In the calculated curves, the additional 13–20 C-terminal residues were modeled as helices: if these are modeled in an extended conformation, the resulting $p(r)$ would be similar to the Sx1a(1-267) curve (blue) but would drop off below the Sx1a(1-267) curve at r ∼80 Å, extend further along r, crossing Sx1a(1-267) at r ∼110 Å, and slowly approaching $p(r) = 0$ at the maximum dimension of the molecule. The experimentally derived MW is consistent with a 1:1 complex, so the conclusion from this analysis is that the experimental shape profile of bound Sx1a(1-261)-His differs

Legend continued on following page

significantly from that of closed Sx1a in the crystal structure. This comparison highlights why modeling Sx1a (and Sx4) against the SAXS and SANS data only yields open conformations. (*B*) Crosslinks between Munc18c (blue) and Sx4 (pink) are shown on a closed binding mode modeled from the Munc18-1:Sx1a crystal structure. Cross-links used in modeling are in blue; those not used in modeling, indicating flexibility of H3, are in red. (*C*) Three cross-links between Munc18-1 (blue) and Sx4 (pink) are shown mapped onto the closed Munc18-1:Sx1a crystal structure; all three were included as restraints in the rigid-body modeling. The scale bar shows 27 Å, the Cα-Cα distance of chemically crosslinked lysines. Distances longer than this indicate incompatibility with the closed binding mode.

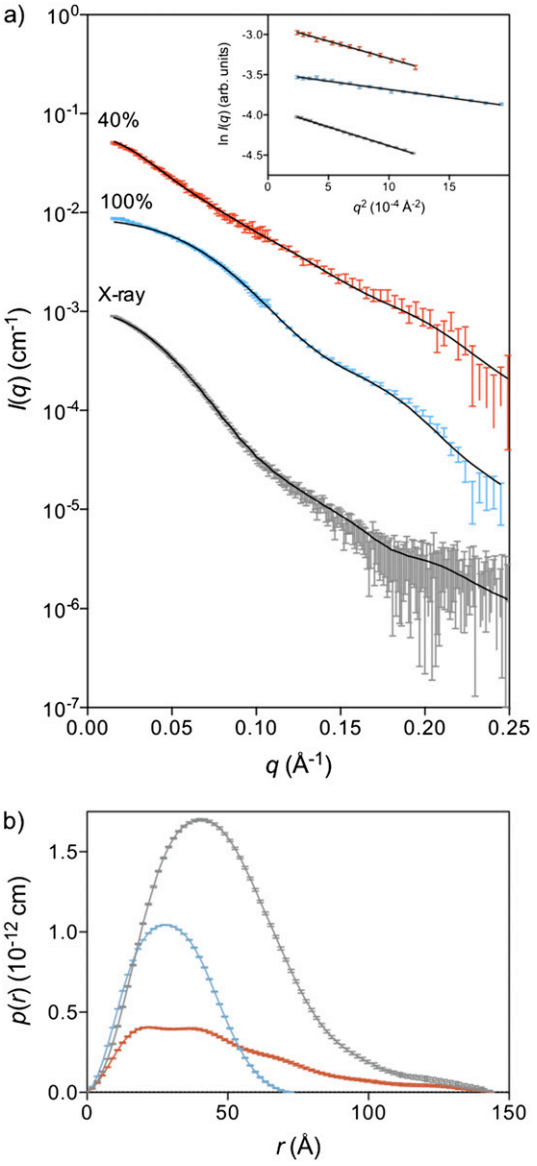

Fig. S4. SAXS and SANS data for Munc18c:Sx4. (*A*) SAXS data (gray) and neutron contrast variation data at 40% D_2O (red; Sx4 dominates scattering) and 100% D_2O (light blue; Munc18c dominates scattering) for Munc18c:Sx4. Data are of high quality with linear Guinier regions (*Inset*) and yielding estimated molecular masses consistent with a 1:1 complex (Table S2). The calculated scattering profiles for the optimized model of the complex (solid lines) are overlaid on the data, showing an excellent correspondence (40%: χ^2 1.0; 100%: χ^2 4.3; χ^2 0.6). Data are shown on an absolute scale, where the 100% and X-ray scattering data have been off-set by factors of 10^{-1} and 10^{-2} for clarity. Error bars represent propagated counting statistics. (*B*) Pair-distance distribution function, $p(r)$, derived from the scattering data using the program GNOM (1).

1. Svergun DI (1992) Determination of the regularization parameter in indirect-transform methods using perceptual criteria. *J Appl Cryst* 25:495–503.

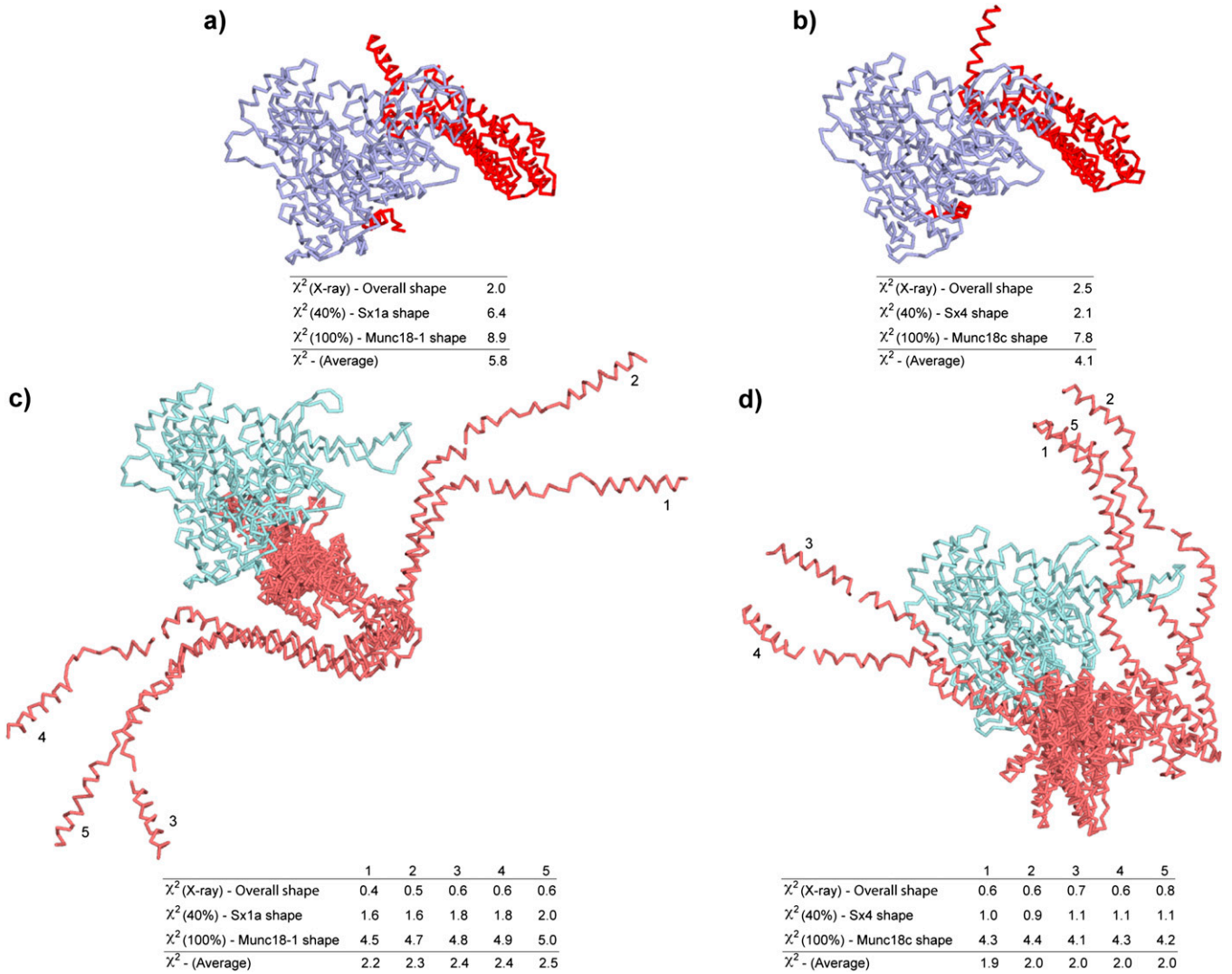

χ^2 (X-ray) - Overall shape	2.0
χ^2 (40%) - Sx1a shape	6.4
χ^2 (100%) - Munc18-1 shape	8.9
χ^2 - (Average)	5.8

χ^2 (X-ray) - Overall shape	2.5
χ^2 (40%) - Sx4 shape	2.1
χ^2 (100%) - Munc18c shape	7.8
χ^2 - (Average)	4.1

	1	2	3	4	5
χ^2 (X-ray) - Overall shape	0.4	0.5	0.6	0.6	0.6
χ^2 (40%) - Sx1a shape	1.6	1.6	1.8	1.8	2.0
χ^2 (100%) - Munc18-1 shape	4.5	4.7	4.8	4.9	5.0
χ^2 - (Average)	2.2	2.3	2.4	2.4	2.5

	1	2	3	4	5
χ^2 (X-ray) - Overall shape	0.6	0.6	0.7	0.6	0.8
χ^2 (40%) - Sx4 shape	1.0	0.9	1.1	1.1	1.1
χ^2 (100%) - Munc18c shape	4.3	4.4	4.1	4.3	4.2
χ^2 - (Average)	1.9	2.0	2.0	2.0	2.0

Fig. S5. Range of models. (*A*) Closed structure of Munc18-1:Sx1a complex (Munc18-1 shown in blue; Sx1a in red) and its associated fit with the scattering data. (*B*) Closed model structure of Munc18c:Sx4 (Munc18c shown in blue; Sx4 in red) based on the Munc18-1:Sx1a crystal structure and its associated fit with the scattering data. (*C*) Best five Munc18-1:Sx1a models, as judged by the average χ^2 and the associated fit to the scattering data (Munc18-1 shown in light cyan; Sx1a in salmon). Models were aligned by superimposing Munc18-1. The orientation of Munc18-1 is the same as in *A*. (*D*) Best five Munc18c:Sx4 models (as judged by the average χ^2) and the associated fit to the scattering data (Munc18c shown in light cyan; Sx4 in salmon). Models were aligned by superimposing Munc18c. The orientation of Munc18c is the same as in *B*. The χ^2 values alone do not provide an objective measure of the quality of the model, but relative comparison of χ^2 values between two models gives an indication of whether one model provides a significantly better representation of the data over the other.

Table S1. Thermodynamic parameters for Munc18-Sx interactions

	Method	ΔH (kcal/mol)	$-T\Delta S$ (kcal/mol)	ΔG (kcal/mol)	K_d (nM)	N	Reference
Munc18-1:Sx1a							
Sx1a(1-261)-His	ITC	−20.6 ± 0.9	8.5 ± 0.8	−12.0 ± 0.1	1.4 ± 0.2	0.98 ± 0.02	This work
His-Sx1a(1-262)	ITC	−34.6 ± 0.2	(22.6)	(−12.0)	1.4 ± 0.3	1.03	(1)
His-Sx1a(1-267) (pQE9 vector)	ITC	−22.1 ± 0.2	(11.2)	(−10.9)	10.0 ± 0.5	1.01	(1)
Sx1a(1-261)	ITC	−35.2 ± 0.2	(23.2)	(−12.0)	1.7 ± 1.2	1.06	(1)
Sx1a(2-243)	ITC	−20.0 ± 0.8	9.6 ± 1.0	−10.4 ± 0.2	27 ± 8	1.05 ± 0.01	(2)
Sx1a(2-243)	ITC	—	—	(−10.8)	7.5 ± 2.7	—	(3)
Munc18-1:Sx1aΔN							
Sx1a(25-261)-His	ITC	−12.0 ± 0.4	1.1 ± 0.5	−11.0 ± 0.2	10 ± 3	1.05 ± 0.09	This work
His-Sx1a(25-262)	ITC	−25.1 ± 0.2	(14.1)	(−11.0)	8.1 ± 1.0	1.01	(1)
Sx1a(2-243)*	ITC	−14.2 ± 0.2	3.8 ± 0.3	−10.4 ± 0.11	26 ± 5	0.96 ± 0.01	(2)
Munc18c:Sx4							
Sx4(1-275) -His	ITC	−7.70 ± 0.1	−1.9 ± 0.1	−9.5 ± 0.1	95 ± 15	0.98 ± 0.02	This work
Sx4(1-273)-GST	SPR	—	—	(−10.3)	28	—	(4)
Sx4(1-273) (amine coupling)	SPR	—	—	(−10.2)	32	—	(5)
Munc18c:Sx4ΔN							
Sx4(30-275)	ITC	No binding detected	—	—	—	—	This work
GST-Sx4(1-273)	SPR	—	—	(−8.9)	254	—	(4)

Residue numbers and N- or C-fusion tags are indicated for the Sxs used in these experiments. Values in brackets were calculated from information provided in the paper reporting the original data. Our finding that Sx4 binds only in an open conformation to Munc18c contradicts earlier conclusions that Munc18c interacts with a closed conformation of Sx4 (4). In those studies, an assumption was made that adding an N-terminal GST fusion tag to Sx4 would abolish the N-peptide binding mode, although the N-peptide was still present in the construct, so that data measured using GST-Sx4 were assumed to represent binding of Sx4 in a closed conformation. However, this assumption ignores the possibility that the observed affinity values could reflect reduced affinity and on and off rates of Munc18c for the tagged Sx4 in an open conformation. We propose that the most appropriate way to investigate the role of N-peptide binding is to delete the N-peptide residues entirely from the Sx rather than modifying the interaction by mutation or fusion. SPR, surface plasmon resonance.
*In this experiment, Munc18-1(F115E/E132A) mutant was used, which is predicted to interfere with Sx1a N-peptide binding. — indicates data not available.

1. Burkhardt P, Hattendorf DA, Weis WI, Fasshauer D (2008) Munc18a controls SNARE assembly through its interaction with the syntaxin N-peptide. *EMBO J* 27:923–933.
2. Malintan NT, et al. (2009) Abrogating Munc18-1-SNARE complex interaction has limited impact on exocytosis in PC12 cells. *J Biol Chem* 284:21637–21646.
3. Deák F, et al. (2009) Munc18-1 binding to the neuronal SNARE complex controls synaptic vesicle priming. *J Cell Biol* 184:751–764.
4. Aran V, et al. (2009) Characterization of two distinct binding modes between syntaxin 4 and Munc18c. *Biochem J* 419:655–660.
5. Jewell JL, Oh E, Bennett SM, Meroueh SO, Thurmond DC (2008) The tyrosine phosphorylation of Munc18c induces a switch in binding specificity from syntaxin 4 to Doc2beta. *J Biol Chem* 283:21734–21746.

Table S2. Concentration series for SAXS data

Concentration (mg/mL)	$I(0)$ (cm^{-1})	$\frac{I(0)}{c \times MW}$
Munc18c:Sx4		
1.40	0.100	7.0
2.60	0.183	6.9
Munc18-1:Sx1a		
1.10	0.075	6.7
2.05	0.144	6.8
3.10	0.210	6.6
Munc18-1:Sx1aΔN		
1.40	0.094	6.7
2.85	0.189	6.6
5.50	0.367	6.7

The measurements show no apparent trend of $I(0)$ normalized by concentration and molecular mass, indicating no significant interparticle interactions.

Table S3. Derived and calculated parameters from scattering data

Complex	Concentration (mg/mL)	R_g (Å)	$I(0)$ (cm^{-1})	D_{max} (Å)	$\Delta\rho$ (10^{10} cm^{-2})	Calculated mass (kDa)
Munc18c: Sx4 solution data						
40% D_2O (Sx4)*	3.0	39.5 ± 0.5	0.1485 ± 0.0012	145	1.45	104
100% D_2O (M18c)†	3.0	23.4 ± 0.3	0.0902 ± 0.0003	70	−1.85	98
X-ray (M18c:Sx4)‡	1.4	38.4 ± 0.3	0.1003 ± 0.0004	145	2.80	102
Munc18-1:Sx1a solution data						
40% D_2O (Sx1a)*	6.6	39.1 ± 0.6	0.1180 ± 0.0010	145	1.40	101
100% D_2O (M18-1)†	2.6	23.7 ± 0.3	0.0864 ± 0.0003	70	−1.90	102
X-ray (M18-1:Sx1a)‡	1.1	37.8 ± 0.3	0.0745 ± 0.0004	145	2.80	96
Munc18-1:Sx1aΔN solution data						
X-ray (M18-1:Sx1aΔN)‡	1.4	33.0 ± 0.3	0.0939 ± 0.0004	100	2.80	95
Munc18-1:Sx1a (closed) crystal structure (calculated values)						
40% D_2O (Sx1a)*	—	32.0	—	110	—	z
100% D_2O (M18-1)†	—	22.5	—	80	—	100
X-ray (M18-1:Sx1a)‡	—	32.9	—	110	—	100

R_g is the radius of gyration of the complex or molecule, $I(0)$ is the forward scattering intensity, and D_{max} is the maximum dimension of the complex or molecule. The contrast values ($\Delta\rho$) were calculated using the program MULCh (1), and the mass of the complex is calculated as described previously (2) using estimates of the concentration, contrast, and forward scattering. — indicates not available.

*Scattering is dominated by deuterium-labeled Sx at the 40% D_2O neutron-scattering contrast point.

†Scattering is dominated by unlabeled Munc18 at the 100% D_2O neutron-scattering contrast point.

‡Scattering is dominated by the Munc18:Sx complex in the X-ray scattering data.

1. Whitten AE, Cai SZ, Trewhella J (2008) MULCh: Modules for the analysis of small-angle neutron contrast variation data from biomolecular assemblies. *J Appl Cryst* 41:222–226.
2. Orthaber D, Bergmann A, Glatter O (2000) SAXS experiments on absolute scale with Kratky systems using water as a secondary standard. *J Appl Cryst* 33:218–225.

Table S4. Cross-linked residues

Cross-link	Linker	Used as <35 Å restraint?	"Closed" distance (Å)
Munc18c:Sx4			
Intramolecular			
Munc18c(K28):Munc18c(K228)	BS3	Yes	
Munc18c(K199):Munc18c(K493)	BS3	No	
Munc18c(K199):Munc18c(K516)	DTSSP	No	
Sx4(M1):Sx4(K44)	DTSSP	Yes	
Intermolecular			
Munc18c(K213):Sx4(K44)	BS3	Yes	53
Munc18c(K315):Sx4(K151)	BS3	Yes	14
Munc18c(K224):Sx4(K267)	BS3	No	63
Munc18c(K278):Sx4(K268)	BS3	No	45
Munc18c(K516):Sx4(K91)	DTSSP	Yes	69
Munc18c(K516):Sx4(K267)	BS3	No	73
Munc18c(T519):Sx4(K64)	BS3	Yes	62
Munc18c(T519):Sx4(K268)	DTSSP	No	80
Munc18-1:Sx1a			
Intramolecular			
Munc18-1(K308):Munc18-1(K321)	BS3	No	11
Munc18-1(K196):Munc18-1(K461)	BS3	No	21
Munc18-1(K264):Munc18-1(K583)	BS3	No	26
Munc18-1(K384):Munc18-1(K465)	BS3	No	24
Sx1a(K12):Sx1a(K117)	BS3	Yes	~40
Sx1a(K46):Sx1a(K117)	BS3	No	23
Sx1a(K55):Sx1a(K126)	BS3	No	19
Sx1a(K12):Sx1a(K126)	BS3	Yes	~43
Intermolecular			
Munc18-1(K125):Sx1a(K12)	BS3	Yes	~15

Intramolecular cross-links were only used in refinement if they were in different rigid domains, as defined in refinement methods. Intermolecular cross-links to Sx4(K267) and Sx4(K268) indicate that H3c samples a variety of conformations. These cross-links, therefore, were not used in refinement; instead, a restraint was added that H3 forms at least one interaction with Munc18. (See *SI Materials and Methods* for more information.) "Closed" distance indicates the distance between equivalent pairs of residues in the Munc18-1:Sx1a(closed) crystal structure (1, 2).

1. Burkhardt P, Hattendorf DA, Weis WI, Fasshauer D (2008) Munc18a controls SNARE assembly through its interaction with the syntaxin N-peptide. *EMBO J* 27:923–933.
2. Misura KMS, Scheller RH, Weis WI (2000) Three-dimensional structure of the neuronal-Sec1-syntaxin 1a complex. *Nature* 404:355–362.